MALDI Mass Spectrometry Imaging of 1-Methyl-4-phenylpyridinium (MPP$^+$) in Mouse Brain

Hanane Kadar · Gael Le Douaron ·
Majid Amar · Laurent Ferrié · Bruno Figadère ·
David Touboul · Alain Brunelle · Rita Raisman-Vozari

Abstract Parkinson's disease (PD) is the second most common neurodegenerative disorder affecting ~ 1 % of the population older than 60 years. The administration of the proneurotoxin 1-methyl-4-phenyl-1,2,3,6-tetrahydropyridine (MPTP) in mice is one of the most widely used approach to elucidate the mechanisms of cell death involved in PD. Its toxicity is attributed to its active metabolite 1-methyl-4-phenylpyridinium (MPP$^+$). However, the magnitude of the PD-like neurodegeneration induced by MPTP depends on many variables, including the route of administration. Different groups, including us, demonstrated that intranasal (i.n.) administration of MPTP constitutes a new route of toxin delivery to the brain that mimics environmental exposure to neurotoxins. In particular, our previous data showed that mice submitted to acute i.n. MPTP administration displayed a significant decrease of striatal dopamine (DA) and a loss of dopaminergic (DA) neurons in the *substantia nigra pars compacta*. However, little is known about the timing and the anatomical distribution of MPP$^+$ after i.n. MPTP administration in mice. In the present study, C57BL/6J mice received one dose of i.n. MPTP (1 mg/nostril) and were sacrificed at two different times after the administration. Using matrix-assisted laser desorption–ionization mass spectrometry imaging, a new technique for the detection of endogenous unlabeled molecules in tissue sections, we showed for the first time the MPP$^+$ anatomical distribution in different brain regions. We demonstrated that the toxin first reached almost all the brain areas; however, in a second time MPP$^+$ remained highly concentrated in the olfactory bulb, the basal ganglia, the ventral mesencephalon, and the *locus coeruleus*, regions differently affected in PD.

H. Kadar · D. Touboul · A. Brunelle (✉)
Centre de Recherche de Gif, Institut de Chimie des
Substances Naturelles, CNRS, Avenue de la Terrasse,
91198 Gif-sur-Yvette Cedex, France
e-mail: alain.brunelle@cnrs.fr

G. Le Douaron · M. Amar · R. Raisman-Vozari
Unité Mixte de Recherche S679, Neurologie et Thérapeutique
Expérimentale, Institut National de la Santé et de la Recherche
Médicale, 47 boulevard de l'Hôpital, 75013 Paris, France

G. Le Douaron · L. Ferrié · B. Figadère
Centre National de la Recherche Scientifique, Laboratoire de
Pharmacognosie, UMR 8076 BioCIS, LabEx LERMIT, Faculté
de Pharmacie, Université Paris-Sud, 5 rue J.B. Clément,
92296 Châtenay-Malabry Cedex, France

Introduction

Parkinson's disease (PD) is the second most common neurodegenerative disorder affecting ~ 1 % of the population older than 60 years. Classically, PD is considered to be a motor system disease and its diagnosis is based on the presence of a set of cardinal motor signs that are the consequence of a pronounced dopaminergic (DA) neuronal cell death in the *substantia nigra pars compacta* (SNpc) and affecting to a lesser extent neurons in the ventral tegmental area (VTA) (Uhl et al. 1985). However, several non-motor symptoms such as cognitive and affective disorders are also commonly observed suggesting that other neurotransmitter systems may be altered (Taylor and Kaiser 1986; Javoy-Agid and Agid 1980). In fact it was

demonstrated that other neurotransmitter systems, e.g., the noradrenergic, cholinergic, and serotoninergic systems, are also involved in PD (Scatton et al. 1983). Dopamine (DA) replacement therapy by L-DOPA is one of the most widely used treatments of PD, offering effective relief of the motor deficits. However, there is no clear result showing that L-DOPA alleviates the non-motor features as well as the underlying DA neuronal degeneration. The development of new therapies in PD depends on the existence of representative animal models to facilitate the evaluation of new pharmacological agents before being applied in clinical trials. Over the years, 1-methyl-4-phenyl-1,2,3,6-tetrahydropyridine (MPTP) has been used with a wide variety of animal species (Kolata 1983; Donnan et al. 1986; Jimenez-Jimenez et al. 1991; Kitamura et al. 1998; Feany and Bender 2000). The administration of MPTP at different doses and given through a number of different routes has led to the development of different versions of the MPTP model. The systemic injection of MPTP is frequently used to intoxicate mice and monkeys damaging the DA nigrostriatal pathway in a pattern similar to that observed in PD (Przedborski et al. 2001). The DA mesocortical pathway is also sensitive to MPTP treatment (Pain et al. 2012). Indeed, MPTP intoxication was associated with frontal cortex DA and noradrenaline loss reported in mice and monkeys (Jackson-Lewis et al. 1995; Pifl et al. 1991; Nayyar et al. 2009). Various studies have reported as well an increase, no change, or a decrease in striatal serotonin (5-HT) concentrations after MPTP treatment (Hallman et al. 1984; Rozas et al. 1998; Vuckovic et al. 2008). Indeed, it was recently shown that 5-HT levels decreased in the midbrain in acute and sub-acute intoxicated mice (Pain et al. 2012).

MPTP by itself is not neurotoxic, but its toxicity is attributed to its active metabolite 1-methyl-4-phenylpyridinium (MPP$^+$). In the brain monoamine oxidase B (MAO-B)-rich cells, especially glial cells (Chiba et al. 1984; Di Monte 2003), oxidize MPTP in its stable toxic metabolite MPP$^+$ (Salach et al. 1984; Dauer and Przedborski 2003). Once formed, MPP$^+$ crosses the glial cell membranes into the extracellular fluid via a yet unknown mechanism and is selectively taken up by DA neurons, inducing mitochondrial dysfunction and nigrostriatal DA denervation. MPP$^+$ is neurotoxic in primates, whereas in rodents only specific strains of mice, particularly C57BL/6J mice, are sensitive (Filipov et al. 2009). Moreover, central DA neurons in mice are differentially susceptible to MPTP neurotoxicity (Behrouz et al. 2007), suggesting possible regional differences in conversion of MPTP–MPP$^+$.

Numerous epidemiological and experimental studies suggest that exposure to agricultural chemicals, viruses, metals, and other toxins contribute to PD pathogenesis (Di Monte 2003; Prediger et al. 2012). In some cases such agents may enter the brain via the olfactory neuroepithelium, a concept termed the olfactory vector hypothesis (Doty 2008). In this context, we have recently proposed a new experimental model of PD consisting of a single intranasal (i.n.) administration of MPTP to rodents. Our findings demonstrated that intranasally MPTP-treated mice suffer from impairments in olfactory and cognitive functions, analogous to those observed during different stages of PD. Such infusion causes time-dependent loss of tyrosine hydroxylase (TH) in the olfactory bulb (OB), the *striatum*, and the SNpc, resulting in significant DA depletion in different brain areas. We also observed a decrease of hippocampal noradrenaline without alterations of the 5-HT system (Prediger et al. 2010).

Identifying precisely the localization of MPP$^+$ in different brain regions would help the understanding of the neurotoxic effect of MPTP on different monoamine neurotransmitters. Although conventional method such as chromatography coupled with mass spectrometry or UV detection has been used for MPP$^+$ quantification after i.n. administration of MPTP (Rojo et al. 2006), this method does not seem to be relevant for determining the anatomical distribution of MPP$^+$ in the brain, since it gives a global amount associated to a structure and cannot describe variations within brain structures. Hence to overcome these drawbacks, matrix-assisted laser desorption–-ionization–time-of-flight (MALDI–TOF) mass spectrometry imaging (MSI) is the technique of choice. In fact, MSI can precisely depict the anatomical distribution of a compound with a lateral resolution of few tens of microns (Caprioli et al. 1997; Cazares et al. 2011; Prideaux and Stoeckli 2012; Castellino et al. 2011; Touboul et al. 2004; McDonnell and Heeren 2007; Setou 2010; Fernandez et al. 2011). Using MALDI MSI this paper thus describes the anatomical distribution of MPP$^+$ in the mouse brain showing that this compound rapidly reaches different brain regions and is especially concentrated in basal ganglia, the ventral mesencephalon (VMS), and the *locus coeruleus* (LC). Furthermore this paper confirms that the nasal route may be used by external neurotoxins to reach the brain to produce neuronal death.

Materials and Methods

Animals

Three-months-old male C57BL/6J mice (R. Janvier, France) were housed, handled, and cared in accordance with the Guide for the Care and Use of Laboratory Animals [National Research Council (NCR) 1996] and the European Union Council Directive 86/609/EEC. Animals were housed and maintained at a constant temperature (22 ± 1 °C) and in a humidity-controlled (55 ± 20 %) environment. A 12/12 h light–dark cycle was kept constant, with lights turned on at

08:00 a.m. During the acclimatization to a new environment period (3 days) and throughout all the study, the animals had free access to food and water.

Intranasal MPTP Intoxication

MPTP–HCl (Sigma-Aldrich, Saint-Quentin-Fallavier, France) was dissolved in 0.9 % NaCl (saline) at a concentration of 100 mg/mL, after which it was acutely administrated by i.n. route to the animals. Briefly, 1 mg of MPTP was inoculated through the nostrils of C57BL/6J mice using a PE-10 micropipette (10 μL solution/nostril), amounting to ~65 mg/kg of MPTP, as previously described (Prediger et al. 2010). Animals were held by the neck and were laid upside down to limit liquid to fall down in the trachea. Control mice were similarly inoculated with saline. Animals were given a 3-min interval to regain normal respiratory function and then this procedure was repeated through the contralateral nostrils. Animals were sacrificed at either 10 or 90 min after MPTP administration. Three groups of animals were used in this study: control group untreated with MPTP (control, $n = 1$); MPTP/10 group ($n = 3$): intranasally infused with MPTP and sacrificed 10 min after the toxin administration; MPTP/90 group ($n = 3$) intranasally infused with MPTP and sacrificed 90 min after the toxin administration.

Tissue Preparation

Ten or ninety minutes after MPTP infusions, mice were anesthetized and perfused transcardially with 25 mL of 1 U/mL heparin in saline, followed by 50 mL of ice-cold buffer to remove traces of blood from the brain and sacrificed by anesthetic overdose (pentobarbital 400 mg/kg, i.p.). Animals were then decapitated and brains were quickly removed. Brains were extracted and sliced into two parts (right and left hemisphere), then snap-frozen in dry-ice-cooled isopentane at −30 °C for 1 min and stored at −80 °C until use. Each frozen brain hemisphere was cut in a para-sagittal plane (medium to lateral) at −20 °C with a cryostat (CM3050-S, Leica Microsystems SA, Nanterre, France). Tissue sections of 14 μm thickness were deposited onto stainless steel plates. For each mouse, brain sections from three different lateral depths (Paxinos and Franklin 2001) (1.32, 0.96, and 0.24 mm) were collected. These depths have been chosen by taking into account specific anatomical regions that may be of interest, because they are involved in PD. The first depths corresponding to 1.32 and 0.96 mm were selected to study the distribution of MPP$^+$ in DA and noradrenergic areas, and the 0.24 mm depth was selected to study the distribution of MPP$^+$ in serotoninergic areas. Each tissue section was examined with an optical microscope (Olympus BX 51 fitted with 1.25× to 50×

lenses, Olympus France SAS, Rungis, France) equipped with a ColorView I camera monitored by Cell^B software (Soft Imaging System GmbH, Münster, Germany). Meanwhile, adjacent sections were also collected on glass slides to perform immunohistochemistry and Nissl staining. These glass slides were stored at −80 °C before being treated.

Before analysis, tissue sections deposited onto stainless steel plates were put under vacuum at a pressure of a few hPa during 10 min to eliminate water from tissue sections. They were then coated with α-cyano-4-hydroxycynamic acid matrix (CHCA), purchased from Sigma-Aldrich (Saint-Quentin-Fallavier, France). Matrix solution was prepared in acetonitrile/water/trifluoroacetic acid (70/30/0.1, v/v/v) at a concentration of 10 mg/mL. Briefly, 50 mg of CHCA was dissolved in 5 mL of solvent. The solution was then vortexed and sonicated, during 5 min each. After being loaded in a 5 mL loop, the matrix was homogeneously sprayed onto the tissue section with a TM-Sprayer (HTX Imaging, Carrboro, NC, USA) in a single coating step. This system is equipped with a nozzle making an aerosol of matrix droplets, by moving above the fixed sample, according to the scheme of the plate loaded in the software. The linear velocity was set at 120 cm/min. The combination of heat (the nozzle temperature is controlled at 70 °C), pressure (carrier solvent at a flow rate of 240 μL/min, high pressure by an isocratic pump), and drying sheath gas (dry nitrogen at a pressure of ~700 hPa) results in a precisely controlled and reproducible solvent/matrix deposition.

MALDI–TOF Mass Spectrometry Imaging

MSI was performed using a 4800 MALDI TOF/TOF mass spectrometer (AB Sciex, Les Ulis, France) equipped with a 200 Hz tripled-frequency Nd/YAG pulsed laser (355 nm) and an electrostatic mirror, leading to a routine mass resolution of about 10,000 in the MS reflectron mode. The data were acquired in the positive ion reflectron mode at an accelerating potential of 20 kV and a delayed extraction time of 200 ns. The number of laser shots per pixel was set at 120 and the distance between two adjacent pixels was fixed at 70 μm, which roughly corresponds to the diameter of the crater formed by ablation onto the tissue surface after 120 laser shots at the same location. Mass spectra were recorded over the mass-to-charge ratio range m/z 100–1,000. External mass calibration was carried out using known lipids and fragments of lipid species like m/z 184.1, 198.1, and 798.5, from another tissue section deposited on the same stainless steel plate. MS images were recorded using the 4000 Series Imaging software (www.maldi-msi.org, M. Stoeckli, Novartis Pharma, Basel, Switzerland) and processed using the TissueView software (AB Sciex, Les

Ulis, France). Some complementary images (Fig. S2) were acquired with an ultrafleXtreme MALDI–TOF/TOF mass spectrometer (Bruker Daltonics, Wissembourg, France) equipped with SmartBeam II Nd/YAG/355 nm laser operating at 1 kHz. For MSI data acquisition, eight accumulations of 100 shots each were summed per pixel and the spatial resolution was fixed to 70 μm. Imaging data acquisitions were performed in reflectron mode under optimized delayed extraction conditions with a source accelerating voltage of 25 kV, in positive polarity. Mass spectra were recorded in the same mass range of m/z 100–1,000 with the same external mass calibration as described above. Image data were acquired with Flex Control v3.3 software and reconstructed/visualized using Flex Imaging v4.0 software (Bruker Daltonics, Wissembourg, France). Although our study in MALDI MSI was not intended to provide quantitative data, it was interesting to investigate potential tissue-specific ion suppression, which could lead to inaccurate variations of MPP^+ ion signal detection. Ion suppression issues are often evaluated when imaging an animal whole body section, since it contains organs with various compositions (Prideaux et al. 2011; Stoeckli et al. 2007). Considering the chemical heterogeneity of the brain structure, it is assumed that extraction efficiency of MPP^+ could differ with the competition of specific endogenous species. A specific control experiment was thus performed in order to evaluate this possible effect. The MPP^+ was purchased from Sigma-Aldrich (Saint-Quentin-Fallavier, France) and prepared at a concentration of 5 ng/μL in a CHCA matrix solution. Thus, a tissue section from a control mouse was homogeneously coated with a mixture of CHCA matrix containing MPP^+, before being analyzed. This concentration was chosen because it led to signal intensities of the same order of magnitude as for the MPP^+ directly desorbed from a treated brain section. Another method of MPP^+ deposition has also been performed to prove the absence of variation of MPP^+ detection due to the tissue composition: a solution of MPP^+ prepared in a mixture of acetonitrile/water/trifluoroacetic acid (70/30/0.1, v/v/v) at a concentration of 5 ng/μL was sprayed onto a tissue sample. The tissue section was then let dry 1 h and coated with a CHCA matrix as previously described in the tissue preparation section, before analysis.

Immunohistochemistry

Immunohistochemistry of tyrosine hydroxylase (TH) (the enzyme that regulates the synthesis of DA) was used for the identification of DA system, and Nissl staining was used for the identification of anatomical brain structures. Staining was performed on 14-μm-thick brain sections collected on glass slides, adjacent to those sections

previously used for MSI analyses. All sections were post-fixed for 15 min in 4 % paraformaldehyde (PFA) solution in phosphate buffer saline (PBS) at 4 °C. For TH immunohistochemistry the sections were rinsed in PBS (0.1 M), endogenous peroxidases and non-specific binding sites were, respectively, blocked with 0.3 % H_2O_2 for 30 min, and with 5 % normal goat serum for 1 h, both diluted in washing buffer. After 3 washing steps, the sections were incubated with rabbit primary antibodies anti-TH (1/500; US Biologicals, Swampscott, MA, USA), diluted in washing buffer containing 0.02 % thimerosal) for 24 h at 4 °C (anti-TH, 1:500, US). Bound antibodies were visualized using biotinylated secondary antibodies (1/250; Vectastain), standard avidin–biotin–peroxidase techniques (1/125; Vectastain Elite ABC kit; Boehringer, Mannheim, Germany), and with 3,3-diaminobenzidine (DAB, Sigma-Aldrich), resulting in a brown color. For the Nissl staining, mouse sections were stained with a thionin solution and the sections were dehydrated in ascending series of ethanol, treated with xylene, and then coversliped. Optical images of TH immunoreactivity were finally acquired by virtual microscopy with NanoZoomer (Hamamatsu, Massy, France) at 0.63×.

Results

MALDI–TOF Mass Spectrometry Imaging for MPP^+ Detection

In order to evaluate a possible ion suppression effect due to the chemical composition of the brain, MPP^+ was homogeneously sprayed on a para-sagittal brain section of an untreated mouse with a TM-Sprayer according to two different methods reported in materials and methods. In MALDI imaging, ion suppression has been assessed either by spraying directly on the tissue the compound of interest spiked in the matrix solution (Hamm et al. 2012; Prideaux et al. 2011) or by spraying the compound first, letting the section dry completely, and then coating it with the matrix (Stoeckli et al. 2007; Pirman et al. 2013). For the first method, an ion signal at m/z 170.1 corresponding to the MPP^+ ion was detected on the brain tissue section (Fig. 1). Figure 1a depicts the MPP^+ ion intensity over the tissue indicating a homogenous distribution of the analyte. In order to get a more reliable measurement, three regions of interest (ROI) of ~ 2 mm^2 each and chosen in three different anatomical areas (Fig. 1b) were drawn and the corresponding mean mass spectra were extracted (Fig. 1c). The average mass spectra of the whole mass range for these three regions (Fig. S1A–C) are also presented, showing a constant signal for all the compounds. In the mass spectrum of Fig. S1D, extracted from the plate, outside of the tissue
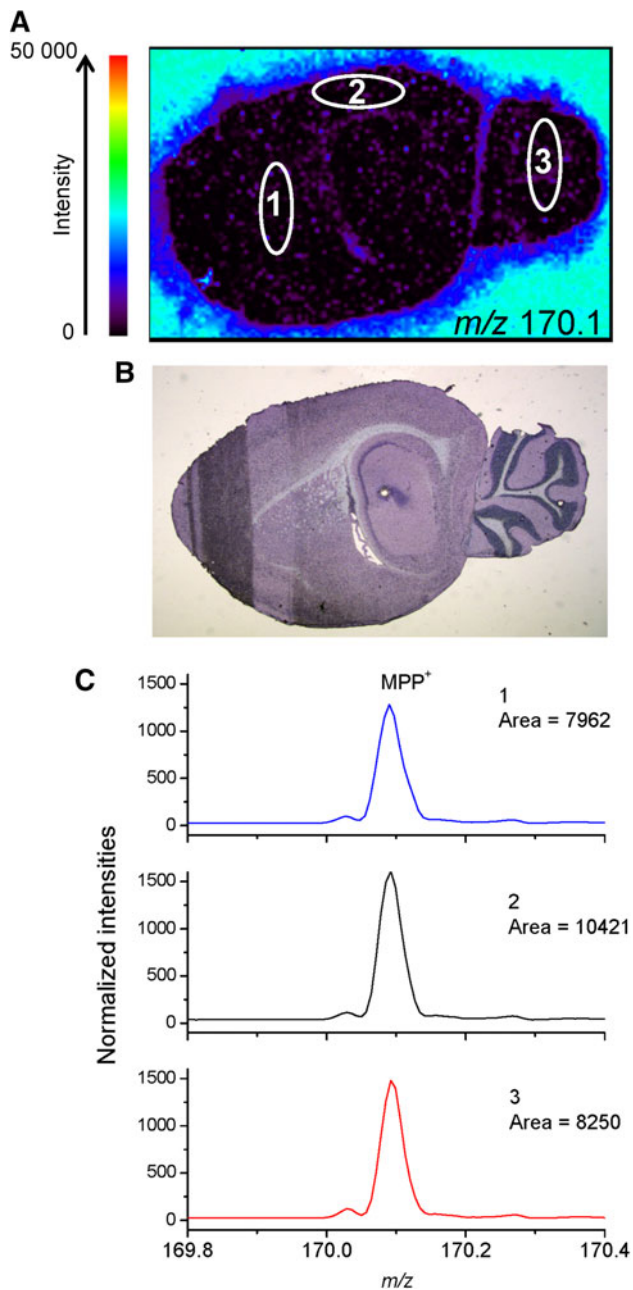
Fig. 1 a MPP$^+$ (*m/z* 170.1) MALDI–TOF ion image of a mouse brain sagittal section coated with a mixture of MPP$^+$ and CHCA matrix with the TM-Sprayer, and regions of interest delimited by the white ellipses. Field of view 9.1 × 4.3 mm, 130 × 82 pixels, pixel size 70 μm. **b** Nissl staining image of the adjacent section to **a** ion image. **c** Mass spectra corresponding to each of the three respective regions of interest

section, the signal is more intense likely because here the surface is conductive. A normalization by a lipid fragment, namely the phosphocholine head group ion signal ([M+H]$^+$, *m/z* 184.1) (Burrell et al. 2007; Fonville et al. 2012) was achieved, leading to the three different spectra presented in Fig. 1c. The obtained relative standard deviation of MPP$^+$ ion peak intensities is about ~15 %,

emphasizing that there is no significant ion suppression effect over the brain section. The second method consisting in the deposition of the MPP$^+$ on the tissue prior to the CHCA coating provides similar results. Figure S2A shows the image obtained with this method of deposition, thus revealing a homogenous MPP$^+$ signal on the entire tissue section. Similar study has been performed to obtain more precise results on the MPP$^+$ intensity variation by selecting three ROI, easily localized by a Nissl staining of an adjacent section (Fig. S2B). Based on the extracted mass spectra (Fig. S2C), variation of the MPP$^+$ ion peak intensities was determined to be ~16 %. The average mass spectra of the whole mass range for the three regions (Fig. S3A–C) showed a constant signal for all the compounds. In the mass spectrum of Fig. S3D, extracted from the plate, outside of the tissue section, the signal is more intense likely because here the surface is conductive. Consequently, the MPP$^+$ ion distribution determined by MALDI–TOF MSI can be used to reliably describe the relative amounts of MPP$^+$ in the different brain areas.

Anatomical Distribution of MPP$^+$ at Different Times After i.n. Administration of MPTP

In order to determine the presence of a brain endogenous compound that could interfere with the signal of the MPP$^+$ ion, we first analyzed the brain of an untreated mouse by MALDI MSI. As expected, no interfering ions were detected in any region of the brain analyzed in three different para-sagittal planes (medium to lateral). The ion image at the same *m/z* value as of MPP$^+$ (Fig. 2a) illustrates this statement. No signal is present on the tissue section. The one appearing on the edge of the control mouse section (Fig. 2) is due to the tail of the isobaric ion present in a highest amount at the exterior of the slice (Fig. S4). An average mass spectrum of the "blank" tissue presented in Fig. 2a was overlaid to an average spectrum of a MPP$^+$-treated tissue presented in Fig. 2b. As shown in Fig. S4, this unknown compound, which is detected in the tissue, is well separated from the signal of interest. In order to avoid the images extracted from the spectra to be affected by this isobaric ion, the integration is performed as described in Fig. S5. The mean mass spectra of each area containing MPP$^+$ are also shown in supplementary materials to support the images (Figs. S6–S9).

To investigate the distribution of the MPP$^+$ ion accumulated in the brain at two different times after a unique i.n. intoxication with 65 mg/kg of MPTP, the brains from mice sacrificed at either 10 or 90 min after intoxication were analyzed by MALDI MSI (Fig. 2b, c, respectively). These experiments were achieved in triplicates for each animal on a similar para-sagittal anatomical level (plane 0.96 mm from Paxinos Atlas) in which different neuronal
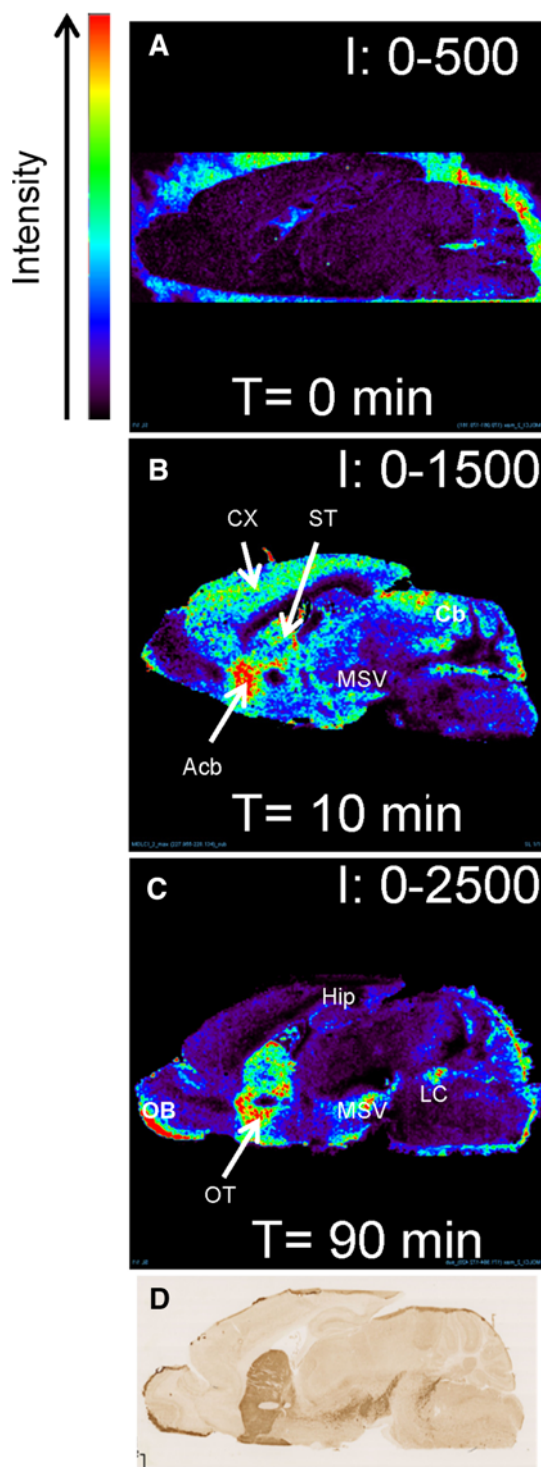
Fig. 2 MALDI–TOF ion images of MPP$^+$ ion (m/z 170.1) at the surface of mouse brain sagittal sections of a non-treated mouse (**a**) or a MPTP intranasally intoxicated mouse and sacrificed at two different times (**b** MPTP/10: intranasally infused with MPTP and sacrificed 10 min after the administration of the toxin and **c** MPTP/90: intranasally infused with MPTP and sacrificed 90 min after the administration of the toxin) at the same para-sagittal plane 0.96 mm from Paxinos Atlas. Field of view 15.4 × 5.6 mm, 220 × 80 pixels, pixel size 70 μm. **d** Tyrosine hydroxylase immunohistochemistry image of sections adjacent to **a**, **b**, and **c** ion images

systems affected in PD could be identified. By overlaying TH$^+$ immunohistochemistry (Fig. 2d) and ion images, the detection of MPP$^+$ ion was precisely attributed to the different DA and noradrenergic anatomical brain areas.

Surprisingly, MPP$^+$ ion was detected in almost the entire MPTP/10 brain, and particularly in OB, *striatum, nucleus accumbens, cerebellum, cortex, hippocampus, LC*, and VMS including: SNpc, *substantia nigra pars reticulata* (SNpr), and VTA (Fig. 2b). In contrast most of the MPP$^+$ ions were concentrated in DA areas, particularly in the *striatum, nucleus accumbens*, and VMS including SNpc, SNpr, and VTA, in the MPTP/90 brain. Other regions like the OB, hippocampus, and the LC also showed accumulation of MPP$^+$ ions. Compared to the MPTP/10 group, MPP$^+$ ion is almost not detected in the cortex and *cerebellum*.

The same anatomical distributions of MPP$^+$ signals have been observed for three different animals confirming reproducibility of the results presented in Fig. 2 (data not shown).

Anatomical Distribution of MPP$^+$ at Different Anatomical Levels After i.n. Administration of MPTP

In order to better understand the toxic effect of MPTP on different monoaminergic systems affected in PD-like DA, noradrenergic and serotoninergic, we analyzed the anatomical distribution of MPP$^+$ ion at 90 min after i.n. administration in two additional para-sagittal planes (para-sagittal plane 0.24 containing 5-HT neurons of the raphe nucleus and 1.32 mm containing the DA system). Time of 90 min after MPTP intoxication was chosen because at that time the highest concentration of MPP$^+$ was previously reported (Rojo et al. 2006).

Results presented in Fig. 3a showed the absence of MPP$^+$ ions in the raphe regions identified in Fig. 3b. Nissl staining of adjacent sections (Fig. 3b) and Paxinos Atlas (Paxinos and Franklin 2001) were used to confirm the anatomical areas. Only OB showed a high density of MPP$^+$ ion. Figure 3c confirms the accumulation of MPP$^+$ at the level of the DA system clearly delimitated by the labeling of TH on the adjacent brain section (Fig. 3d). Similar to Fig. 2c, MPP$^+$ ion was detected in the *striatum, nucleus accumbens, olfactory tubercle*, OB, and *hippocampus*.

Discussion

MALDI–TOF Mass Spectrometry Imaging for MPP$^+$ Detection

It is commonly admitted that raw data of MSI experiments acquired with MALDI–TOF cannot be directly used for semi-quantitative measurements since the desorption–ionization may depend on the biological and chemical
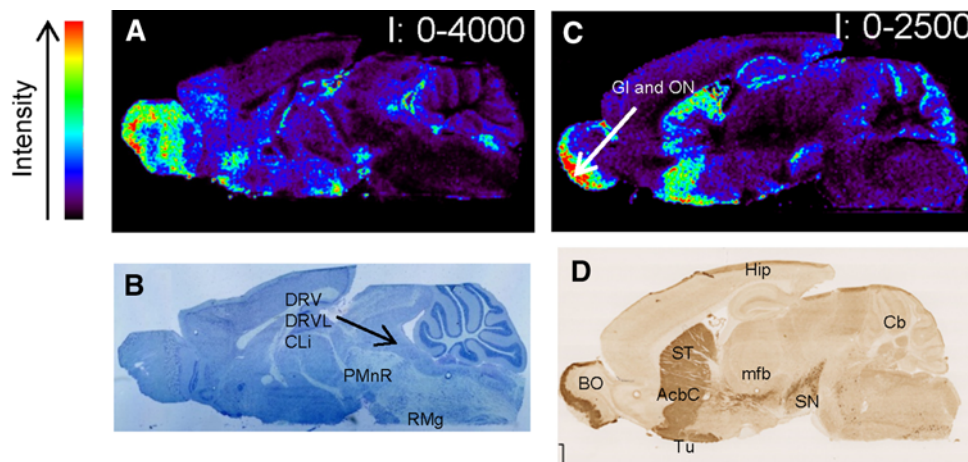
Fig. 3 Images of mouse brain sagittal sections (two different lateral depths) from mice treated with an i.n. dose of MPTP and sacrificed 90 min after the administration of the toxin: **a**, **b** 0.24 mm and **c**, **d** 1.32 mm. **a**, **c** MALDI–TOF positive ion images of MPP$^+$ ion (*m/z* 170.1). Field of view 15.4 × 7.1 mm, 102 × 218 pixels, pixel size 70 μm. **b** Nissl staining images of section adjacent to **a** ion images. **d** Tyrosine hydroxylase immunohistochemistry image of section adjacent to **c** ion images

environment. This is what is called an ion suppression effect or sometimes a matrix effect: various factors including matrix layer heterogeneity, variation in desorption or ionization efficiency, or ion suppression or enhancement on different tissue regions (Fernandez et al. 2011) may induce variations of the ion signal. Some of these sources of error, such as variation in sample preparation, are nowadays considerably reduced, thanks to the homogeneous coating ensured by robotic instruments. For instance, the TM-sprayer, which is used in this study, has been largely implemented for MSI experiments for its reliability and robustness (Cerruti et al. 2011; Mainini et al. 2011; Brignole-Baudouin et al. 2012). After normalization by the intensity of a lipid fragment ion (Burrell et al. 2007; Fonville et al. 2012), the absence of matrix effect for MPP$^+$ ion desorption, ionization, or detection has been verified. Another widely used type of normalization based the total total ion current (TIC) (Sugiura and Setou 2009; Norris et al. 2007) has also been tested and led to similar results. Table S1 shows the comparison between the two normalization methods.

MPP$^+$ Distribution

Using MALDI MSI, a recent and innovative technique permitting the localization of molecular ions at the surface of tissue sections, we described for the first time the anatomical distribution of MPP$^+$ in different mice brain regions after the i.n. administration of MPTP.

Among several other different methods, TOF–SIMS (Touboul et al. 2011), nano-SIMS (Guerquin-Kern et al. 2005), DESI (Girod et al. 2011), and LA-ICP-MS (Becker et al. 2010), which have respective advantages and

drawbacks in terms of sensitivity, lateral resolution, and robustness, MALDI MSI is the prominent one in bioanalytical studies, and offers an excellent sensitivity, together with a spatial resolution in the range of tens of micrometer (McDonnell and Heeren 2007; Setou 2010; Fernandez et al. 2011). It is used for various applications in pharmaceutical research (Castellino et al. 2011; Brignole-Baudouin et al. 2012), biomarker discovery (Touboul et al. 2004, 2007; Bakry et al. 2011), and biomedical research (Touboul et al. 2005; Benabdellah et al. 2009; Gemoll et al. 2011).

It is known that i.n. MPTP was transformed into the toxin MPP$^+$ (Rojo et al. 2006; Chiba et al. 1984), and our results showed that MPP$^+$ reached rapidly multiple sites within the brain ~10 min after administration. The analyzed para-sagittal brain sections indicated the presence of MPP$^+$ in several anatomical structures, including OB, cortex, *hippocampus*, *nucleus accumbens*, *striatum*, VMS, *cerebellum*, *thalamus*, and *hypothalamus*. The presence of MPP$^+$ ion in the OB was previously reported by Rojo et al. (2006) using a LC–UV method, without providing precise information on the spatial distribution in this brain structure. Conversely, MALDI MSI gives the precise spatial distribution, allowing the MPP$^+$ localization in para-sagittal plane 0.24 and 1.32 mm both in the olfactory nerve (ON) layer and the glomerular layer (Gl) by comparison with the mouse atlas (Paxinos and Franklin 2001).

The olfactory region of the nasal passages has anatomic and physiological characteristics that provide both extracellular and intracellular pathways into the CNS to substances bypassing the blood–brain barrier (Broadwell et al. 1988; Thorne et al. 1995; Illum 2000). A direct extracellular pathway between the nasal passages and the brain was first conclusively demonstrated for the tracer horseradish

peroxidase (HRP), which i.n. administered passed freely through intercellular junctions of the olfactory epithelia to rapidly reach the OB of the CNS (within minutes) (Broadwell et al. 1988). Rapid delivery, as fast as 5–10 min in some cases, of therapeutics to the brain has been demonstrated with a variety of i.n. delivered drugs, confirming the importance of this extracellular transport mechanism (Chen et al. 2012).

This rapid speed of transport suggests that for many compounds extracellular convection along the olfactory and trigeminal nerves accounts for a significant portion of i.n. delivery to the CNS (Lochhead and Thorne 2012). An intracellular pathway from the nasal passages to the brain is a more slow process (Broadwell and Balin 1985). A transneuronal distribution of tracers was observed in the olfactory tubercle, in the piriform cortex, and also in neurons of the basal forebrain, a major source of cholinergic afferents to the OB. These results suggested that the olfactory system provide a route of entry for exogenous substances to the basal forebrain (Baker and Spencer 1986). In addition, it has recently been suggested that the rostral migratory stream, which is the pathway used by neuronal progenitors to migrate from periventricular regions to the OB, may also play a role in the delivery of molecules from the nasal cavity to the brain (Scranton et al. 2011).

The rapid nature of MPTP delivery into the CNS from the nasal passages, showed in the present study, is most consistent with the transport of the toxin by an extracellular route along components of the peripheral olfactory and trigeminal systems as previously described for IGF-I (Thorne et al. 2004). Although the blood–brain barrier does not alter the arriving to the brain of substances administrated intranasally, it can be difficult to totally avoid some systemic exposure with an intranasally delivered small lipophilic molecule like MPTP (Chapman et al. 2012).

Results showed that 90 min after i.n. MPTP intoxication, its toxic metabolite MPP$^+$ was concentrated specifically in the OB, *striatum*, *accumbens*, olfactory tubercles, VMS, *hippocampus*, and *LC*. Interestingly, most of these brain regions contain higher density of the catecholamine transporters (Javitch and Snyder 1984; Fuller and Steranka 1985) that participate to the intracellular transport of MPP$^+$ into the neurons in which it will induce neuronal death, specially the DA system (Prediger et al. 2010). Indeed, the accumulation of MPP$^+$ in the *hippocampus* and the *LC* observed in the present study could be linked to the noradrenaline decrease previously reported in the *hippocampus* by our group after i.n. MPTP intoxication (Prediger et al. 2012). Differences in the density of monoamine uptake sites and/or turnover of monoamine transporters might explain differences in the accumulation of MPP$^+$ between 10 and 90 min after i.n. MPTP (Buck and Amara 1994; Pifl et al. 1996).

The sequestration at sites of retention could be a dominant mechanism compared to the more general distribution of the toxin observed at 10 min representing probably a continuous influx at sites of entry. A study performed with monkeys by Herkenham et al. (1991) showed that the *striatum* had a far more prolonged retention time for MPP$^+$ if compared to the cortex, the *LC*, or the *substantia nigra* themselves. They thus correlated differences in sensitivity among brain areas with ex vivo MPP$^+$ levels.

However, not all the regions that concentrated MPP$^+$ showed a similar effect on DA system. The *accumbens* was indeed less affected than the *striatum* by MPTP (Boeckler et al. 2003) and our results showed a higher density of MPP$^+$ in the *accumbens* than in the *striatum* as previously reported by Lehner et al. (2011). The consequence of the accumulations remains to be clarified, since it was previously reported that a significant increase in the amount of striatal MPP$^+$ did not always produce an effect on striatal DA levels (Fornai et al. 1996). Apart from the different mechanisms of action that could account for these results, our data, as previously proposed by Vaglini et al. (1996), are in contrast with the current belief that a direct relationship exists between MPP$^+$ concentrations and the degree of MPTP-induced depletion of DA.

Although the precise mechanisms underlying nose to brain transport remain incompletely understood (Merkus et al. 2003), i.n. administration is associated with several advantages (non-invasiveness, ease of application, and avoidance of hepatic first-pass elimination) that encourages its use as a good strategy for delivering toxins like MPTP into the CNS to study neuronal death processes.

The peripherally administered MPTP neurotoxin is converted into MPP$^+$ not only by MAO-B in astrocytes (Vila et al. 2001) but also by endothelial cells of the blood vessels. The brain origin of MPP$^+$ after i.n. administration of MPTP remains, however, to be clearly determined.

An important conclusion of this study is that the contact with environmental neurotoxins may constitute a risk factor for brain diseases because such substances could be very quickly distributed in most of the brain regions, and also concentrated in regions in which a high density of receptors could bind it.

Conclusion

MSI allows for the first time the precise distribution of MPP$^+$ toxin inducing PD in a mouse model. By directly imaging MPP$^+$ in different parts of the brain, this study has demonstrated that the ON pathway could mediate a rapid brain delivery of intranasally administered MPTP. Taken together, these results showed that MPTP intranasal administration provides a good animal model to evaluate new neuroprotective therapies in PD.

References

Baker H, Spencer RF (1986) Trans-neuronal transport of peroxidase-conjugated wheat-germ agglutinin (wga–hrp) from the olfactory epithelium to the brain of the adult-rat. Exp Brain Res 63:461–473. doi:10.1007/bf00237470

Bakry R, Rainer M, Huck CW, Bonn GK (2011) Protein profiling for cancer biomarker discovery using matrix-assisted laser desorption/ionization time-of-flight mass spectrometry and infrared imaging: a review. Anal Chim Acta 690:26–34. doi:10.1016/j.aca.2011.01.044

Becker JSa, Zoriy M, Matusch A, Wu B, Salber D, Palm C, Becker JSu (2010) Bioimaging of metals by laser ablation inductively coupled plasma mass spectrometry (LA-ICP-MS). Mass Spectrom Rev 29:156–175. doi:10.1002/mas.20239

Behrouz B, Drolet RE, Sayed ZA, Lookingland KJ, Goudreau JL (2007) Unique responses to mitochondrial complex I inhibition in tuberoinfundibular dopamine neurons may impart resistance to toxic insult. Neuroscience 147:592–598. doi:10.1016/j.neuroscience.2007.05.007

Benabdellah F, Yu H, Brunelle A, Laprévote O, De La Porte S (2009) MALDI reveals membrane lipid profile reversion in MDX mice. Neurobiol Dis 36:252–258. doi:10.1016/j.nbd.2009.07.013

Boeckler F, Leng A, Mura A, Bettinetti L, Feldon J, Gmeiner P, Ferger B (2003) Attenuation of 1-methyl-4-phenyl-1,2,3,6-tetrahydropyridine (MPTP) neurotoxicity by the novel selective dopamine D-3-receptor partial agonist FAUC 329 predominantly in the nucleus accumbens of mice. Biochem Pharmacol 66:1025–1032. doi:10.1016/s0006-2952(03)00451-9

Brignole-Baudouin F, Desbenoit N, Hamm G, Liang H, Both J-P, Brunelle A, Fournier I, Guérineau V, Legouffe R, Stauber J, Touboul D, Wisztorski M, Salzet M, Laprévote O, Baudouin C (2012) A new safety concern for glaucoma treatment demonstrated by mass spectrometry imaging of benzalkonium chloride distribution in the eye, an experimental study in rabbits. PLoS ONE 7:e50180. doi:10.1371/journal.pone.0050180

Broadwell RD, Balin BJ (1985) Endocytic and exocytic pathways of the neuronal secretory process and transsynaptic transfer of wheat-germ agglutinin–horseradish peroxidase in vivo. J Comp Neurol 242:632–650. doi:10.1002/cne.902420410

Broadwell RD, Balin BJ, Salcman M (1988) Transcytotic pathway for blood-borne protein through the blood–brain barrier. Proc Natl Acad Sci USA 85:632–636

Buck KJ, Amara SG (1994) Chimeric dopamine norepinephrine transporters delineate structural domains influencing selectivity for catecholamines and 1-methyl-4-phenylpyridinium. Proc Natl Acad Sci USA 91:12584–12588. doi:10.1073/pnas.91.26.12584

Burrell MM, Earnshaw CJ, Clench MR (2007) Imaging matrix assisted laser desorption ionization mass spectrometry: a technique to map plant metabolites within tissues at high spatial resolution. J Exp Bot 58:757–763. doi:10.1093/jxb/erl139

Caprioli RM, Farmer TB, Gile J (1997) Molecular imaging of biological samples: localization of peptides and proteins using MALDI–TOF MS. Anal Chem 69:4751–4760. doi:10.1021/ac970888i

Castellino S, Groseclose MR, Wagner D (2011) MALDI imaging mass spectrometry: bridging biology and chemistry in drug development. Bioanalysis 3:2427–2441. doi:10.4155/bio.11.232

Cazares LH, Troyer DA, Wang B, Drake RR, Semmes OJ (2011) MALDI tissue imaging: from biomarker discovery to clinical applications. Anal Bioanal Chem 401:17–27. doi:10.1007/s00216-011-5003-6

Cerruti CD, Touboul D, Guerineau V, Petit VW, Laprévote O, Brunelle A (2011) MALDI imaging mass spectrometry of lipids by adding lithium salts to the matrix solution. Anal Bioanal Chem 401:75–87. doi:10.1007/s00216-011-4814-9

Chapman DC, Frey WH, Craft S, Danielyan L, Hallschmid M, Schiöth HB, Benedict C (2012) Intranasal treatment of central nervous system dysfunction in Humans. Pharm Res 30:2475–2484. doi:10.1007/s11095-012-0915-1

Chen J, Zhang C, Liu QF, Shao XY, Feng CC, Shen YH, Zhang QZ, Jiang XG (2012) Solanum tuberosum lectin-conjugated PLGA nanoparticles for nose-to-brain delivery: in vivo and in vitro evaluations. J Drug Target 20:174–184. doi:10.3109/1061186x.2011.622396

Chiba K, Trevor A, Castagnoli N (1984) Metabolism of the neurotoxic tertiary amine, MPTP, by brain monoamine-oxidase. Biochem Biophys Res Commun 120:574–578. doi:10.1016/0006-291x(84)91293-2

Dauer W, Przedborski S (2003) Parkinson's disease: mechanisms and models. Neuron 39:889–909. doi:10.1016/s0896-6273(03)00568-3

Di Monte DA (2003) The environment and Parkinson's disease: is the nigrostriatal system preferentially targeted by neurotoxins? Lancet Neurol 2:531–538. doi:10.1016/S1474-4422(03)00501-5

Donnan GA, Kaczmarczyk SJ, Solopotias T, Rowe P, Kalnins RM, Vajda FJ, Mendelsohn FA (1986) The neurochemical and clinical effects of 1-methyl-4-phenyl-1,2,3,6-tetrahydropyridine in small animals. Clin Exp Neurol 22:155–164

Doty RL (2008) The olfactory vector hypothesis of neurodegenerative disease: is it viable? Ann Neurol 63:7–15. doi:10.1002/ana.21327

Feany MB, Bender WW (2000) A Drosophila model of Parkinson's disease. Nature 404:394–398. doi:10.1038/35006074

Fernandez JA, Ochoa B, Fresnedo O, Giralt MT, Rodriguez-Puertas R (2011) Matrix-assisted laser desorption ionization imaging mass spectrometry in lipidomics. Anal Bioanal Chem 401:29–51. doi:10.1007/s00216-011-4696-x

Filipov NM, Norwood AB, Sistrunk SC (2009) Strain-specific sensitivity to MPTP of C57BL/6 and BALB/c mice is age dependent. Neuroreport 20:713–717. doi:10.1097/WNR.0b013e32832aa95b

Fonville JM, Carter C, Cloarec O, Nicholson JK, Lindon JC, Bunch J, Holmes E (2012) Robust data processing and normalization strategy for MALDI mass spectrometric imaging. Anal Chem 84:1310–1319. doi:10.1021/ac201767g

Fornai F, Bassi L, Torracca MT, Allessandri MG, Scalori V, Corsini GU (1996) Region- and neurotransmitter-dependent species and strain differences in DSP-4-induced monoamine depletion in rodents. Neurodegeneration 5:241–249. doi:10.1006/neur.1996.0032

Fuller RW, Steranka LR (1985) Central and peripheral catecholamine depletion by 1-methyl-4-phenyl-tetrahydropyridine (MPTP) in rodents. Life Sci 36:243–247. doi:10.1016/0024-3205(85)90066-9

Gemoll T, Roblick UJ, Habermann JK (2011) MALDI mass spectrometry imaging in oncology (review). Mol Med Rep 4:1045–1051. doi:10.3892/mmr.2011.566

Girod M, Shi YZ, Cheng JX, Cooks RG (2011) Mapping lipid alterations in traumatically injured rat spinal cord by desorption electrospray ionization imaging mass spectrometry. Anal Chem 83:207–215. doi:10.1021/ac102264z

Guerquin-Kern JL, Wu TD, Quintana C, Croisy A (2005) Progress in analytical imaging of the cell by dynamic secondary ion mass spectrometry (SIMS microscopy). Biochim Biophys Acta 1724:228–238. doi:10.1016/j.bbagen.2005.05.013

Hallman H, Olson L, Jonsson G (1984) Neurotoxicity of the meperidine analog N-methyl-4-phenyl-1,2,3,6-tetrahydropyridine on brain

catecholamine neurons in the mouse. Eur J Pharmacol 97: 133–136. doi:10.1016/0014-2999(84)90521-1

Hamm G, Bonnel D, Legouffe R, Pamelard F, Delbos JM, Bouzom F, Stauber J (2012) Quantitative mass spectrometry imaging of propranolol and olanzapine using tissue extinction calculation as normalization factor. J Proteomics 75:4952–4961. doi:10.1016/j.jprot.2012.07.035

Herkenham M, Little MD, Bankiewicz K, Yang SC, Markey SP, Johannessen JN (1991) Selective retention of MPP$^+$ within the monoaminergic systems of the primate brain following MPTP administration—an in vivo autoradiographic study. Neuroscience 40:133–158. doi:10.1016/0306-4522(91)90180-v

Illum L (2000) Transport of drugs from the nasal cavity to the central nervous system. Eur J Pharm Sci 11:1–18. doi:10.1016/s0928-0987(00)00087-7

Jackson-Lewis V, Jakowec M, Burke RE, Przedborski S (1995) Time-course and morphology of dopaminergic neuronal death caused by the neurotoxin 1-methyl-4-phenyl-1,2,3,6-tetrahydropyridine. Neurodegeneration 4:257–269. doi:10.1016/1055-8330(95)90015-2

Javitch JA, Snyder SH (1984) Uptake of MPP(+) by dopamine neurons explains selectivity of parkinsonism-inducing neurotoxin, MPTP. Eur J Pharmacol 106:455–456. doi:10.1016/0014-2999(84)90740-4

Javoy-Agid F, Agid Y (1980) Is the mesocortical dopaminergic system involved in Parkinson disease? Neurology 30:1326–1330. doi:10.1212/WNL.30.12.1326

Jimenez–Jimenez FJ, Tabernero C, Mena MA, Deyebenes JG, Deyebenes MJG, Casarejos MJ, Pardo B, Garciaagundez JA, Benitez J, Martinez A, Garciaasenjo AL (1991) Acute effects of 1-methyl-4-phenyl-1,2,3,6-tetrahydropyridine in a model of rat designated a poor metabolizer of debrisoquine. J Neurochem 57:81–87. doi:10.1111/j.1471-4159.1991.tb02102.x

Kitamura Y, Kakimura J, Taniguchi T (1998) Protective effect of talipexole on MPTP-treated planarian, a unique Parkinsonian worm model. Jpn J Pharmacol 78:23–29. doi:10.1254/jjp.78.23

Kolata G (1983) Monkey model of Parkinson's disease. Science 220:705. doi:10.1126/science.6403987

Lehner A, Johnson M, Simkins T, Janis K, Lookingland K, Goudreau J, Rumbeiha W (2011) Liquid chromatographic-electrospray mass spectrometric determination of 1-methyl-4-phenylpyridine (MPP+) in discrete regions of murine brain. Toxicol Mech Methods 21:171–182. doi:10.3109/15376516.2010.538753

Lochhead JJ, Thorne RG (2012) Intranasal delivery of biologics to the central nervous system. Adv Drug Deliv Rev 64:614–628. doi:10.1016/j.addr.2011.11.002

Mainini V, Angel PM, Magni F, Caprioli RM (2011) Detergent enhancement of on-tissue protein analysis by matrix-assisted laser desorption/ionization imaging mass spectrometry. Rapid Commun Mass Spectrom 25:199–204. doi:10.1002/rcm.4850

McDonnell LA, Heeren RMA (2007) Imaging mass spectrometry. Mass Spectrom Rev 26:606–643. doi:10.1002/mas.20124

Merkus P, Guchelaar HJ, Bosch A, Merkus F (2003) Direct access of drugs to the human brain after intranasal drug administration? Neurology 60:1669–1671. doi:10.1212/01.WNL.0000067993.60735.77

Nayyar T, Bubser M, Ferguson MC, Neely MD, Goodwin JS, Montine TJ, Deutch AY, Ansah TA (2009) Cortical serotonin and norepinephrine denervation in parkinsonism: preferential loss of the beaded serotonin innervation. Eur J Neurosci 30:207–216. doi:10.1111/j.1460-9568.2009.06806.x

Norris JL, Cornett DS, Mobley JA, Andersson M, Seeley EH, Chaurand P, Caprioli RM (2007) Processing MALDI mass spectra to improve mass spectral direct tissue analysis. Int J Mass Spectrom 260:212–221. doi:10.1016/j.ijms.2006.10.005

Pain S, Gochard A, Bodard S, Gulhan Z, Prunier-Aesch C, Chalon S (2012) Toxicity of MPTP on neurotransmission in three mouse models of Parkinson's disease. Exp Toxicol Pathol 65:689–694. doi:10.1016/j.etp.2012.09.001

Paxinos G, Franklin KBJ (2001) The mouse brain in stereotaxic coordinates, 2nd edn. Academic Press, San Diego

Pifl C, Schingnitz G, Hornykiewicz O (1991) Effect of 1-methyl-4-phenyl-1,2,3,6-tetrahydropyridine on the regional distribution of brain monoamines in the rhesus-monkey. Neuroscience 44:591–605. doi:10.1016/0306-4522(91)90080-8

Pifl C, Hornykiewicz O, Giros B, Caron MG (1996) Catecholamine transporters and 1-methyl-4-phenyl-1,2,3,6-tetrahydropyridine neurotoxicity: studies comparing the cloned human noradrenaline and human dopamine transporter. J Pharmacol Exp Ther 277:1437–1443

Pirman DA, Reich RF, Kiss A, Heeren RMA, Yost RA (2013) Quantitative MALDI tandem mass spectrometric imaging of cocaine from brain tissue with a deuterated internal standard. Anal Chem 85:1081–1089. doi:10.1021/ac302960j

Prediger RDS, Aguiar AS, Rojas-Mayorquin AE, Figueiredo CP, Matheus FC, Ginestet L, Chevarin C, Del Bel E, Mongeau R, Hamon M, Lanfumey L, Raisman-Vozari R (2010) Single intranasal administration of 1-methyl-4-phenyl-1,2,3,6-tetrahydropyridine in C57BL/6 mice models early preclinical phase of Parkinson's disease. Neurotox Res 17:114–129. doi:10.1007/s12640-009-9087-0

Prediger RDS, Aguiar AS Jr, Matheus FC, Walz R, Antoury L, Raisman-Vozari R, Doty RL (2012) Intranasal administration of neurotoxicants in animals: support for the olfactory vector hypothesis of Parkinson's disease. Neurotox Res 21:90–116. doi:10.1007/s12640-011-9281-8

Prideaux B, Stoeckli M (2012) Mass spectrometry imaging for drug distribution studies. J Proteomics 75:4999–5013. doi:10.1016/j.jprot.2012.07.028

Prideaux B, Dartois V, Staab D, Weiner DM, Goh A, Via LE, Barry CE, Stoeckli M (2011) High-sensitivity MALDI-MRM-MS imaging of moxifloxacin distribution in tuberculosis-infected rabbit lungs and granulomatous lesions. Anal Chem 83:2112–2118. doi:10.1021/ac1029049

Przedborski S, Chen QP, Vila M, Giasson BI, Djaldatti R, Vukosavic S, Souza JM, Jackson-Lewis V, Lee VMY, Ischiropoulos H (2001) Oxidative post-translational modifications of alpha-synuclein in the 1-methyl-4-phenyl-1,2,3,6-tetrahydropyridine (MPTP) mouse model of Parkinson's disease. J Neurochem 76:637–640. doi:10.1046/j.1471-4159.2001.00174.x

Rojo AI, Montero C, Salazar M, Close RM, Fernandez-Ruiz J, Sanchez-Gonzalez MA, de Sagarra MR, Jackson-Lewis V, Cavada C, Cuadrado A (2006) Persistent penetration of MPTP through the nasal route induces Parkinson's disease in mice. Eur J Neurosci 24:1874–1884. doi:10.1111/j.1460-9568.206.05060.x

Rozas G, Liste I, Guerra MJ, Labandeira-Garcia JL (1998) Sprouting of the serotonergic afferents into striatum after selective lesion of the dopaminergic system by MPTP in adult mice. Neurosci Lett 245:151–154. doi:10.1016/s0304-3940(98)00198-0

Salach JI, Singer TP, Castagnoli N, Trevor A (1984) Oxidation of the neurotoxic amine 1-methyl-4-phenyl-1,2,3,6-tetrahydropyridine (MPTP) by monoamine oxidase-a and oxidase-b and suicide inactivation of the enzymes by MPTP. Biochem Biophys Res Commun 125:831–835. doi:10.1016/0006-291x(84)90614-4

Scatton B, Javoy-Agid F, Rouquier L, Dubois B, Agid Y (1983) Reduction of cortical dopamine, noradrenaline, serotonin and their metabolites in Parkinson's disease. Brain Res 275:321–328. doi:10.1016/0006-8993(83)90993-9

Scranton RA, Fletcher L, Sprague S, Jimenez DF, Digicaylioglu M (2011) The rostral migratory stream plays a key role in intranasal delivery of drugs into the CNS. PLoS ONE 6:018711. doi:10.1371/journal.pone.0018711

Setou M (ed) (2010) Imaging mass spectrometry. Springer, Dordrecht. doi:10.1007/978-4-431-09425-8

Stoeckli M, Staab D, Schweitzer A (2007) Compound and metabolite distribution measured by MALDI mass spectrometric imaging in whole-body tissue sections. Int J Mass Spectrom 260:195–202. doi:10.1016/j.ijms.2006.10.007

Sugiura Y, Setou M (2009) Selective imaging of positively charged polar and nonpolar lipids by optimizing matrix solution composition. Rapid Commun Mass Spectrom 23:3269–3278. doi:10.1002/rcm.4242

Taylor JW, Kaiser ET (1986) The structural characterization of beta-endorphin and related peptide-hormones and neurotransmitters. Pharmacol Rev 38:291–319

Thorne RG, Emory CR, Ala TA, Frey WH (1995) Quantitative-analysis of the olfactory pathway for drug-delivery to the brain. Brain Res 692:278–282. doi:10.1016/0006-8993(95)00637-6

Thorne RG, Pronk GJ, Padmanabhan V, Frey WH (2004) Delivery of insulin-like growth factor-I to the rat brain and spinal cord along olfactory and trigeminal pathways following intranasal administration. Neuroscience 127:481–496. doi:10.1016/j.neuroscience.2004.05.029

Touboul D, Piednoël H, Voisin V, De La Porte S, Brunelle A, Halgand F, Laprévote O (2004) Changes in phospholipid composition within the dystrophic muscle by matrix-assisted laser desorption/ionization mass spectrometry and mass spectrometry imaging. Eur J Mass Spectrom 10:657–664. doi:10.1255/ejms.671

Touboul D, Brunelle A, Halgand F, De La Porte S, Laprévote O (2005) Lipid imaging by gold cluster time-of-flight secondary ion mass spectrometry: application to Duchenne muscular dystrophy. J Lipid Res 46:1388–1395. doi:10.1194/jlr.M500058-JLR200

Touboul D, Roy S, Germain DP, Chaminade P, Brunelle A, Laprévote O (2007) MALDI–TOF and cluster–TOF–SIMS imaging of Fabry disease biomarkers. Int J Mass Spectrom 260:158–165. doi:10.1016/j.ijms.2006.09.027

Touboul D, Laprévote O, Brunelle A (2011) Micrometric molecular histology of lipids by mass spectrometry imaging. Curr Opin Chem Biol 15:725–732. doi:10.1016/j.cbpa.2011.04.017

Uhl G, Hedreen JC, Price DLMD (1985) Parkinson's disease: loss of ineurons from the ventral tegmental area contralateral to therapeutic surgical lesions. Neurology 35:1215–1218

Vaglini F, Fascetti F, Tedeschi D, Cavalletti M, Fornai F, Corsini GU (1996) Striatal MPP$^+$ levels do not necessarily correlate with striatal dopamine levels after MPTP treatment in mice. Neurodegeneration 5:129–136. doi:10.1006/neur.1996.0019

Vila M, Jackson-Lewis V, Guegan C, Wu DC, Teismann P, Choi DK, Tieu K, Przedborski S (2001) The role of glial cells in Parkinson's disease. Curr Opin Neurol 14:483–489. doi:10.1097/00019052-200108000-00009

Vuckovic MG, Wood RI, Holschneider DP, Abernathy A, Togasaki DM, Smith A, Petzinger GM, Jakowec MW (2008) Memory, mood, dopamine, and serotonin in the 1-methyl-4-phenyl-1,2,3,6-tetrahydropyridine-lesioned mouse model of basal ganglia injury. Neurobiol Dis 32:319–327. doi:10.1016/j.nbd.2008.07.015